

Submitted to: *The Astronomical Journal*

CH 3 GHz Observations of Molecular Clouds Along the Galactic Plane

Loris Magnani and Samantha Lugo

Department of Physics and Astronomy, The University of Georgia, Athens, GA 30602
loris@physast.uga.edu

and

T. M. Dame

Harvard-Smithsonian Center for Astrophysics, 60 Garden St., MS 72, Cambridge, MA 02138

ABSTRACT

Spectra in the CH ${}^2\Pi_{1/2}$, $J=1/2$, $F=1-1$ transition at 3335 MHz were obtained in three 5-point crosses centered on the Galactic plane at $\ell = 50^\circ$, 100° , and 110° . The lines of sight traverse both Giant Molecular Clouds (GMCs) and local, smaller entities. This transition is a good tracer of low-density molecular gas and the line profiles are very similar to CO(1-0) data at nearly the same resolution. In addition, the CH 3335 MHz line can be used to calibrate the CO-H₂ conversion factor (X_{CO}) in low-density molecular gas. Although this technique underestimates X_{CO} in GMCs, our results are within a factor of two of X_{CO} values calibrated for GMCs by other techniques. The similarity of CH and CO line profiles, and that of X_{CO} values derived from CH and more traditional techniques, implies that most of the molecular gas along the observed lines of sight is at relatively low densities ($n \leq 10^3 \text{ cm}^{-3}$).

Subject headings: Galaxy: surveys, ISM: molecules, radio lines: ISM

1. Introduction

The CH ground state, hyperfine, main line (${}^2\Pi_{1/2}$, $J = 1/2$, $F = 1-1$) at 3335 MHz is a good, though seldom used, tracer of low-density molecular gas ($n \sim 10^2 - 10^3 \text{ cm}^{-3}$ - Magnani

et al. 2003 and references therein). One of the earliest surveys of the CH 3 GHz lines¹ by Rydbeck et al. (1976) detected emission from all the denser types of molecular clouds: Giant Molecular Clouds (GMCs), dark clouds, and what today would be referred to as translucent clouds. The CH 3 GHz lines are nearly ubiquitous in molecular gas detectable via the CO(1-0) line. Unfortunately, the CH lines tend to be very weak, with peak antenna temperatures that seldom surpass 0.5 K and, more often, are in the tens of milliKelvin range. This is partly a consequence of the relatively low CH abundance (compared to CO) in interstellar clouds as determined from observations (4×10^{-8} with respect to H₂; e.g., Liszt & Lucas (2002) and reference therein), and partly because of the peculiar non-thermal excitation of the 3 GHz transitions (e.g., Rydbeck et al. 1976; Liszt & Lucas 2002). However, the linear relationship of N(CH) with N(H₂) - at least for $N(H_2) < 5 \times 10^{21} \text{ cm}^{-2}$ (Federman 1982; Danks, Federman, & Lambert 1984; Mattila 1986; Rachford et al. 2002, Liszt & Lucas 2002; Magnani et al. 2003; Weselak et al. 2004) - makes CH a valid tracer of molecular gas in all but the densest cloud regions (which tend to occupy little cloud volume - see below) and, because the transition is optically thin in the interstellar medium, many of the difficulties inherent in interpreting CO(1-0) data are avoided.

The only systematic CH survey of the Galactic plane was made by Johansson (1979) and his results, though intriguing, are not well-known because they were published in a report of the Research Laboratory of Electronics and Onsala Space Observatory. Basically, the Galactic plane was surveyed in the CH 3335 MHz line at 2.5° or 5° intervals from $\ell = 10^\circ$ - 230°. Like the CO emission, the CH peaks at a galactocentric distance of 5.5 kpc (assuming $R_\odot = 10$ kpc) and the equivalent of the Molecular Ring (e.g., Scoville & Sanders 1987; Dame, Hartmann, & Thaddeus 2001; Simon et al. 2001) is clearly seen in the CH data. However, in comparison with to the CO distribution, the CH data show significant excess emission between 7 - 10 kpc. Given that the CH distribution in this portion of the Galaxy appeared to be intermediate between the CO and HI distributions, Johansson (1979) speculated that a portion of the CH emission arose from a low-density molecular gas regime that was not readily traceable by CO. The existence of such a regime has sometimes been proposed to explain infrared excess regions (e.g., Reach, Wall, & Odegard 1998; Blitz, Bazell, & Désert 1990).

The question of whether the CH 3335 MHz line can trace low-density H₂ not detectable in the CO(1-0) transition has been explored in some detail by Magnani & Onello (1993; 1995) and revisited by Magnani et al. (2003). The consensus opinion seems to be that deep CO spectra will generally reveal the same lines as seen in deep CH spectra. The CO surveys used

¹The $^2\Pi_{1/2}$, $J = 1/2$ lambda-doubling transition consists of 3 hyperfine structure components: The $F = 1-1$ main line at 3335 MHz, and the $F = 0-1$ and $1-0$ satellite lines at 3264 and 3349 MHz, respectively.

by Johansson (1979) may not have been sufficiently sensitive to pick up the CO equivalent of the excess CH emission between 7-10 kpc. However, regardless of the ultimate resolution of the excess CH issue, the results of Johansson (1979) merit further consideration.

In addition to confirming the Johansson (1979) results, CH observations of the 3335 MHz line can be used to calibrate the CO-H₂ conversion factor, $X_{\text{CO}} [\equiv N(\text{H}_2)/W_{\text{CO}}$, where W_{CO} is the velocity-integrated CO(1-0) antenna temperature]. Magnani & Onello (1995) find that this method works well for translucent molecular gas but is thought to break down for dark molecular clouds and for the denser portions of GMCs. The principal reason is that in dense (and thus opaque) molecular regions, CH is converted into more complex molecular species so that its abundance decreases rapidly with increasing $N(\text{H}_2)$, n , or opacity (e.g., Federman 1982; Viala 1986; Lee, Bettens, & Herbst 1996; Liszt & Lucas 2002). In addition to chemistry considerations, the presence of significant background continuum radiation (from HII regions embedded in GMCs) can also drive down the CH antenna temperature (Rydbeck et al. 1976).

Observations compiled from several sources by Mattila (1986) confirm this result; in using $N(\text{CH})$ as a molecular tracer for 6 GMC lines of sight underestimates $N(\text{H}_2)$ significantly (see Figure 10 of his paper). However, even if CH completely disappeared at high densities, GMCs are not uniformly at $n > 10^3 \text{ cm}^{-3}$. The molecular envelopes around dense, star-forming cores have low enough densities and constitute enough of the cloud to drive the average molecular volume density of GMCs down to 50 cm^{-3} (Blitz 1991). Lada, Bally, & Stark (1991) estimate from CO observations that the dense cores (i.e., those with $n \geq 10^4 \text{ cm}^{-3}$) in the L1630 (Orion B) GMC constitute only a small fraction (not greater than 19%) of the total cloud mass. The fraction of a GMC's mass and volume as a function of n likely varies greatly from cloud to cloud and has not been adequately studied. Nevertheless, GMC envelopes around dense cores are ideal sources for the CH 3 GHz lines and the early CH surveys confirmed this [Rydbeck et al. (1976); Hjalmarson et al. (1977); Genzel et al. (1979)]², although the CH lines were often weaker than those observed in dark clouds. However, because of the decreased abundance of CH at high molecular densities, the CH 3335 MHz line will systematically underestimate $N(\text{H}_2)$ and, thus, X_{CO} in GMCs. The key issue is to determine how significant is this effect.

In order to examine these issues further, we conducted a preliminary CH Galactic plane survey with the NRAO 140 ft telescope, observing CH emission from 4 regions along the Galactic plane. Three of the regions were centered at $b = 0^\circ$ and $\ell = 50^\circ$, 100° , and 110° ,

²In many star-forming regions, the CH 3264 MHz satellite line is stronger than the main line at 3335 MHz because of far-infrared pumping from HII regions - see Rydbeck et al. (1976).

and are described in this paper; the other region covered the Galactic Center and, given its uniqueness and exclusion from the Johansson (1979) survey, the observations are described elsewhere (Magnani et al. 2005). In §2 of this paper, we describe the set-up for the CH 3335 MHz and C¹⁸O 109.8 GHz observations, and the results are presented in §3. In §4, we discuss the CH - H₂ relation at higher N(H₂) than usual and, in §5, derive the values of X_{CO} for the various components along the observed lines of sight. A brief conclusion closes the paper.

2. Observations

The CH 3335 line was observed in 3 general directions along the Galactic plane in 1999 March using the now-defunct 140 ft telescope in Green Bank, West Virginia. At 3.3 GHz the beam size of the 140 ft was 9'. The observing configuration consisted of a front end with a corrugated dual-hybrid mode feed in which two linear polarizations were fed into a dual-channel FET amplifier receiver. The system temperature on the sky ranged from 35 - 50 K, depending on the atmospheric conditions and the antenna elevation. The autocorrelator was configured into two sections of 512 channels, with each section covering a bandwidth of 5 MHz at a velocity resolution of 0.88 km s⁻¹ per channel. The total velocity coverage of each spectrum was \sim 450 km s⁻¹ centered on the v_{LSR} velocity corresponding to the bulk of the CO emission as determined from the Dame, Hartmann, & Thaddeus (2001) survey.

A 5-point cross was made at each of the 3 locations with the central spectrum at $b = 0^\circ$ and $\ell = 50^\circ$, 100° , and 110° , and the other 4 spectra offset by 0.125° in latitude or longitude. Each position was observed in ON-OFF mode with one hour total on-source integrations. The OFF positions were typically 10° away from the plane in b . For each line of sight, the two polarizations were added together and the resulting spectrum was baselined with a polynomial of order 6 and Hann smoothed to yield an *rms* noise level of \sim 5-8 mK. Individual reduced spectra for the 5 positions centered on $(\ell, b) = (50^\circ, 0^\circ)$ are shown in Figures 1a - 1e along with the corresponding CO(1-0) spectra from the Dame, Hartmann, & Thaddeus (2001) Galactic survey. The CO data are at comparable angular and velocity resolution (8.8' and 0.65 or 1.3 km s⁻¹, respectively). For $(\ell, b) = (110^\circ, 0^\circ)$, only the central position is shown in both CH and CO in Figure 2 (there is little change in the spectra from one position to another in this region), and for $(\ell, b) = (100^\circ, 0^\circ)$, both the CH and CO signals were relatively weak so that all 5 spectra are summed together to make a single composite spectrum shown in Figure 3.

The three central positions ($\ell = 50^\circ$, 100° , and 110° at $b = 0^\circ$) were also observed in the C¹⁸O(1-0) line at 109.8 GHz with the CfA 1.2 meter telescope, the same instrument used

for the Dame et al. (2001) CO survey. Flat spectral baselines were obtained by position switching every 15 s between the source position and two emission-free positions chosen to straddle the source in elevation. Residual baseline offsets (< 1 K) were removed by fitting straight lines to the baseline region. At 109.8 GHz, the 256 channel filterbank spectrometer provided a velocity resolution of 0.68 km s^{-1} over a range of 174 km s^{-1} . Total integration times per position ranged from 1 to 3 hours, yielding rms noise levels of 12 - 16 mK per channel.

3. Results

The CH and CO profiles shown in Figures 1-3 are strikingly similar to each other. Everywhere there is CO(1-0) emission there is also CH emission. However, the integration times are very different. Each CH spectrum was observed for at least one-hour on source, whereas the CO spectra were only observed for a few minutes. Although the CH spectra presented in this paper have significantly higher signal-to-noise ratios than the Johansson (1979) results (5-8 mK vs. 20 mK), nevertheless, the spectra for equivalent lines of sight look quite similar (the resolution of the data in this paper is $9'$ vs. $15'$ for the Johansson data).

All the spectra centered on $(\ell, b) = (50^\circ, 0^\circ)$ and the composite spectrum at $(\ell, b) = (100^\circ, 0^\circ)$ show two or more components whose velocity was assigned using the antenna temperature-weighted velocity over the extent of each spectral feature. We treat each velocity component as a separate spectral feature. In table 1, columns 1 and 2 list the observed position, column 3 shows the antenna temperature-weighted velocity of the component, and column 4 the velocity-integrated CH antenna temperature (defined to be W_{CH}) for each of the 21 velocity components. From W_{CH} , the column density can be obtained in the traditional manner (see Rydbeck et al. 1976) using the formula:

$$N(\text{CH}) = 2.82 \times 10^{11} [\eta_f \eta_b (T_{ex} - T_{bg})]^{-1} T_{ex} W_{\text{CH}} \text{ cm}^{-2} \quad (1)$$

where T_{ex} and T_{bg} are the excitation and background temperatures respectively, η_f is the filling fraction of CH in the telescope beam (assumed to be 1 for the observations described in this paper), η_b is the beam efficiency (0.79 at 3335 MHz for the 140-ft telescope - Ron Maddalena, private communication), and W_{CH} is measured in mK km s^{-1} . Because T_{ex} is usually negative and $|T_{ex}| \gg T_{bg}$ for the 3 GHz lines (Genzel et al. 1979; Hjalmarson et al. 1977; Rydbeck et al. 1976), the quantity in square brackets is nearly always close to unity (however, see discussion in Magnani & Onello 1995 and Liszt & Lucas 2002). Consequently,

$N(CH)$ is directly proportional to W_{CH} and is tabulated in column 5 of Table 1.

Once $N(CH)$ has been obtained, the conversion to $N(H_2)$ follows from the empirical relation established by Mattila (1986):

$$N(H_2) = (2.1 \times 10^7)N(CH) + 2.2 \times 10^{20} \quad cm^{-2} \quad (2)$$

However, as pointed out in the §1, this empirical relation is calibrated only for values of $N(H_2) < 5 \times 10^{21} \text{ cm}^{-2}$. Nevertheless, the values obtained by using equation 2 are listed in column 6 of Table 1.

4. The $N(CH)$ - $N(H_2)$ Relation

As Figures 1-3 make clear, the CH 3335 MHz spectral line profiles track the CO(1-0) emission, and thus H_2 , very well; at all velocities where there is CO(1-0) emission, there is also CH emission - albeit at a much lower antenna temperature. This is confirmed by plotting W_{CH} vs. W_{CO} ; the linear relation that ensues has a correlation coefficient of 0.76. However, in order to compare our results with earlier work, we convert W_{CH} to $N(CH)$ via equation 1, and W_{CO} to $N(H_2)$ using the standard Galactic plane value of X_{CO} ($1.6 \times 10^{20} \text{ cm}^{-2} \text{ K km s}^{-1}$ - Hunter et al. 1987). The plot of $\log N(CH)$ vs. $\log N(H_2)$ is very similar to what was obtained by Mattila (1986) and is shown in Figure 4. It is clear from the figure that the lines of sight with the greatest $N(H_2)$ tend to deviate from the Mattila relation. Thus, $N(CH)$ appears to systematically underestimate $N(H_2)$ for values $> 5 \times 10^{21} \text{ cm}^{-2}$. However, it is important to stress that, in this regime, the $N(H_2)$ values derived from CO observations may have large uncertainties associated with them. $N(H_2)$ is not directly determined, and statements of how any quantity varies with $N(H_2)$ in dense molecular regions must be viewed with some caution.

A least squares fit to our data yields $N(H_2) = 3.60 \times 10^7 N(CH) - 2.36 \times 10^{20}$, somewhat similar equation 2. If we fit only those points in our data set with $N(H_2) < 5 \times 10^{21}$, we obtain a best fit line $N(H_2) = 2.46 \times 10^7 N(CH) + 1.47 \times 10^{20}$, virtually identical to the Mattila result.

Liszt & Lucas (2002) combine translucent and dark cloud CH and CO data from Magnani & Onello (1995) and new CH and CO observations to create an $N(CH)$ vs. W_{CO} plot that shows three modes of behavior: (1) A slow increase of $N(CH)$ with W_{CO} is evident for both dark and translucent gas. (2) A nearly fixed, factor of 3 offset in the best fit lines to the dark vs. translucent data sets, with the dark data having the larger y-intercept. (3) A

scatter in $N(CH)$ at any given value of W_{CO} ascribed by Liszt and Lucas to variations in the CH excitation and the local physical conditions.

The second point is somewhat problematic because the data for MBM16 from Magnani & Onello (1995) are classified by Liszt & Lucas (2002) as belonging to the dark cloud category. MBM16 is a translucent cloud according to the standard definition of translucent: $1 \leq A_V \leq 5$ magnitudes (van Dishoeck & Black 1988). Direct measurements of the cloud extinction by the method of star counts conducted by Magnani & de Vries (1986) indicate that the average extinction of the cloud is only 0.9 magnitudes (A_V) above the background with even the most obscured regions barely above 2 magnitudes. Nevertheless, it is possible that the CH excitation conditions in MBM16 differ enough from those in “normal” translucent gas that the CH and CO properties of this object may be more similar to those found in dark molecular gas. Assuming that the bimodal distribution attributed to the data by Liszt & Lucas (2002) does indeed exist, and is not merely a large scatter in the CH and CO properties of the clouds, Liszt and Lucas speculate that the shallowness of the slope in the diffuse gas reflects the trend that at low extinction $N(CO) \propto [N(CH)]^2 \propto [N(H_2)]^2$. In the dark gas, the same shallow slope (albeit with a y-intercept a factor of 3 higher) likely reflects the decline of the CH abundance in denser gas at higher values of W_{CO} .

In Figure 5, following Liszt & Lucas (2002), we present a plot of $N(CH)$ vs. W_{CO} for our data (star symbols). Also included in the plot are the data Liszt & Lucas classify as arising from dark and translucent gas (plotted as diamond symbols and plus signs, respectively). As is clear from the figure, the Galactic plane data fall on and extend the relationship for the dark clouds noted by Liszt & Lucas (2002). Thus, the Galactic plane molecular clouds observed in this paper are as likely underabundant in CH as the dark cloud population selected by Liszt & Lucas (2002).

5. The Value of X_{CO} in Giant Molecular Clouds

Magnani & Onello (1995) describe in detail how to derive X_{CO} using CH 3335 MHz and CO 115 GHz data. In essence, equations 1 and 2 are used to obtain $N(H_2)$ from the CH data, and this result is divided by W_{CO} at similar resolution to immediately yield X_{CO} . This was done for all 21 components in our sample and the results are tabulated in Table 2 and shown graphically in Figure 6.

The lines of sight centered on and around $(\ell, b) = (50^\circ, 0^\circ)$ typically show 3 separate components: a relatively weak feature at $\sim 6 \text{ km s}^{-1}$ that likely arises from very local, small, molecular clouds, and stronger emission from Inner Galaxy GMCs at $v_{LSR} \sim 45$ and 57 km

s^{-1} . This interpretation is confirmed by Figure 7a which shows the $\text{C}^{18}\text{O}(1-0)$ spectrum for $(\ell, b) = (50^\circ, 0^\circ)$. This transition traces dense molecular gas typically found in the cores of GMCs or dark clouds ($n > 10^4 \text{ cm}^{-3}$), and is detected for this line of sight only at $v_{\text{LSR}} \sim 45$ and 57 km s^{-1} . The average X_{CO} for the 6 km s^{-1} gas is 1.9×10^{20} , while the Inner Galaxy X_{CO} values are somewhat lower; 1.2×10^{20} and 1.3×10^{20} for the 45 and 57 km s^{-1} features, respectively. These relatively low values of X_{CO} may be the result of the CH method underestimating the true value of $N(\text{H}_2)$ in GMCs, as discussed above. However, if the correct value of X_{CO} in these Inner Galaxy regions is obtained from the standard 1.6×10^{20} value used by Hunter et al. (1997), the CH method underestimates $N(\text{H}_2)$ and, consequently, X_{CO} , by no more than a factor of 2.

The lines of sight centered on and around $(\ell, b) = (100^\circ, 0^\circ)$ have only one component at $v_{\text{LSR}} \sim -50 \text{ km s}^{-1}$ that arises from molecular clouds in the Perseus spiral arm. The C^{18}O spectrum from the central position shows relatively strong emission at $v_{\text{LSR}} \sim -50 \text{ km s}^{-1}$ (see Figure 7b) indicating that the molecular gas along this line of sight has a dense component. The values of X_{CO} derived using the CH method produce values of X_{CO} ranging from $0.5 - 1.5 \times 10^{20}$ with an average of 0.8×10^{20} . Again, these determinations most likely underestimate the real values. However, as in the case of Inner Galaxy GMCs, the underestimate is not severe; no more than a factor of 2-3.

The 5-point cross centered on $b = 0^\circ$ and $\ell = 100^\circ$ has a much lower W_{CO} than the other two regions, and the CH 3335 MHz line is also so weak that the 5 lines of sight have to be averaged in order to identify the two components (see Figure 3). In contrast to the preceding two regions, the corresponding values of X_{CO} derived from the CH data are larger than the standard values by factors of 3 and 9, seemingly implying that the CH method may be overestimating $N(\text{H}_2)$ for these lines of sight. However, it is more likely given the weakness of the CO and CH lines in the direction $(\ell, b) = (100^\circ, 0^\circ)$ that this emission is not tracing molecular gas in GMCs or dark cloud complexes but, rather, molecular gas in lower density, lower opacity objects such as translucent clouds. In support of this conclusion, the C^{18}O spectrum for the central position shows no signal to an rms of 16 mK. In these types of clouds, X_{CO} can vary by more than an order of magnitude from cloud to cloud and even over a single cloud, and can take on values both substantially higher and lower than the standard value (Magnani & Onello 1995; Magnani et al. 1998).

For those lines of sight with W_{CO} values greater than 10 K km s^{-1} , indicative of the presence of GMCs or other high column and volume density clouds, the X_{CO} values derived from the CH method are systematically lower than the conventional value for the Galactic plane by factors of 2-3. For those lines of sight with W_{CO} more similar to what is expected from somewhat lower column density molecular clouds - like dark clouds, X_{CO} tends to be

close to the conventional value. Finally, for the lines of sight where the two components have W_{CO} values lower than those of dark clouds, more similar to what is seen in translucent molecular gas, the X_{CO} values are larger than normal; typical of what is obtained when using the CH method on translucent clouds (Magnani & Onello 1995).

6. Conclusions

The CH 3335 MHz observations described in this paper confirm that this transition is a good tracer of molecular gas at low densities. Figures 1-3 underscore how strikingly similar CH 3335 MHz profiles can be to CO(1-0) profiles at similar resolution. Although the weakness of the line in most Galactic environments probably precludes its use in large-scale surveys, the result from the undersampled Galactic plane survey made by Johansson (1979) - that there is more molecular gas between the Molecular Ring and the Solar Circle than has been traced by the CO surveys - should probably be revisited. If this gas exists, it can undoubtedly also be traced by the CO(1-0) line, but integration times longer than what has commonly been employed by the large-scale surveys are probably needed.

As first noted by Magnani & Onello (1995), for lower density molecular gas typical of that found in small, local molecular clouds, X_{CO} as determined from the CH method is consistent with other determinations - though variations from cloud to cloud can be significant. For GMCs, the data presented here show that $N(H_2)$ and, consequently, X_{CO} is systematically underestimated by the CH method. This is what would be expected from the chemistry of the molecule as described in §1. Surprisingly, the underestimate is not more than a factor of 2-3 compared to what is obtained from other methods. Given astrochemistry models of dense molecular gas environments, this result implies that most of the volume of GMCs is not at high molecular densities ($n > 10^3 \text{ cm}^{-3}$) and the lower density envelopes contribute significantly to the overall molecular mass (see also, Lada, Bally, & Stark 1991; Blitz, 1991; Magnani, Hartmann, & Speck 1996).

The results described above are limited, covering 21 velocity components distributed over 15 lines of sight along 3 principal directions in the Galactic plane. Unfortunately, the capacity to obtain more data is even more limited. Currently, in the Western Hemisphere, the only radio telescope equipped to make CH 3 GHz observations is at Arecibo. The nature of the Arecibo dish is such that only a limited portion of the Galactic Glane can be surveyed (the Galactic Center is unaccessible with that telescope). Given the promising results from our preliminary survey project, we hope that in the not too distant future the 100 meter NRAO telescope at Green Bank will be outfitted with an upper S-band receiver so that a proper survey might be conducted.

We thank Ben Engebretson for help with some of the observations at the 140-ft telescope and Emily Brown for help with some of the data reduction. We also thank an anonymous referee for comments that improved the presentation.

Table 1. CH Observations and Derived Quantities

ℓ °	b °	component ^a km s ⁻¹	W _{CH} K km s ⁻¹	N(CH) ^b cm ⁻²	N(H ₂) ^c cm ⁻²
49.875	0.000	6.2	0.081	2.89×10^{13}	0.83×10^{21}
		46.0	0.382	1.36×10^{14}	3.08×10^{21}
		59.3	0.258	9.21×10^{13}	2.15×10^{21}
50.000	0.125	6.8	0.161	5.75×10^{13}	1.43×10^{21}
		44.6	0.216	7.71×10^{13}	1.84×10^{21}
		55.5	0.263	9.39×10^{13}	2.19×10^{21}
50.000	0.000	6.7	0.135	4.82×10^{13}	1.23×10^{21}
		45.4	0.424	1.51×10^{14}	3.39×10^{21}
		57.4	0.387	1.38×10^{14}	3.12×10^{21}
50.000	-0.125	4.9	0.184	6.57×10^{13}	1.60×10^{21}
		47.9	0.717	2.56×10^{14}	5.60×10^{21}
		5.9	0.099	3.53×10^{13}	9.61×10^{20}
50.125	0.000	43.7	0.349	1.25×10^{14}	2.84×10^{21}
		55.0	0.306	1.09×10^{14}	2.51×10^{21}
		-5.0	0.139	4.96×10^{13}	1.26×10^{21}
100.000	0.000	-31.4	0.313	1.12×10^{14}	2.57×10^{21}
		-51.0	0.140	5.00×10^{13}	1.27×10^{21}
		109.875	0.000		
110.000	0.125	-50.8	0.200	7.14×10^{13}	1.72×10^{21}
		0.000	0.271	9.67×10^{13}	2.25×10^{21}
		-51.1	0.368	1.31×10^{14}	2.97×10^{21}
110.000	-0.125	-51.6	0.342	1.22×10^{14}	2.78×10^{21}
		-52.8			
110.125	0.000				

^aThe antenna temperature-weighted velocity is given for each spectral component (see Figures 1-3).

^bN(CH) is derived from the integrated antenna temperature in column 4 after correcting for the beam efficiency, the beam filling fraction, and assuming $|T_{ex}| \gg T_{bg}$. See text for details.

^cN(H₂) derived from N(CH) via equation 2 (see text).

Table 2. CH and CO Observations and Derived Quantities for GMCs

ℓ °	b °	component ^a km s ⁻¹	W _{CO} ^b K km s ⁻¹	N(H ₂) ^c cm ⁻²	f ^d	X _{CO} ^e × 10 ²⁰
49.875	0.000	6.2	5.43	0.87 × 10 ²¹	0.95	1.5
		46.0	20.66	3.31 × 10 ²¹	0.93	1.5
		59.3	15.26	2.44 × 10 ²¹	0.88	1.4
50.000	0.125	6.8	12.49	2.00 × 10 ²¹	0.72	1.1
		44.6	12.24	1.96 × 10 ²¹	0.94	1.5
		55.5	23.21	3.72 × 10 ²¹	0.59	0.9
50.000	0.000	6.7	10.97	1.75 × 10 ²¹	0.70	1.1
		45.4	27.20	4.36 × 10 ²¹	0.78	1.2
		57.4	30.09	4.82 × 10 ²¹	0.65	1.0
50.000	-0.125	4.9	7.07	1.13 × 10 ²¹	1.42	2.3
		47.9	52.38	8.38 × 10 ²¹	0.67	1.1
50.125	0.000	5.9	2.88	4.60 × 10 ²⁰	2.09	3.3
		43.7	21.70	3.48 × 10 ²¹	0.82	1.3
		55.0	19.07	3.05 × 10 ²¹	0.82	1.3
100.000	0.000	-5.0	3.18	5.08 × 10 ²⁰	2.48	4.0
		-31.4	1.77	2.84 × 10 ²⁰	9.05	14.5
109.875	0.000	-51.0	8.47	1.35 × 10 ²¹	0.94	1.5
110.000	0.125	-50.8	23.06	3.69 × 10 ²¹	0.47	0.7
110.000	0.000	-51.1	36.18	5.79 × 10 ²¹	0.39	0.6
110.000	-0.125	-51.6	44.09	7.06 × 10 ²¹	0.42	0.7
110.125	0.000	-52.8	51.65	8.27 × 10 ²¹	0.34	0.5

^asame as Table 1

^bIntegrated CO(1-0) line emission from the data of Ungerechts, Hunbanhowar, & Thaddeus (2000); Dame, Hartmann, & Thaddeus (2001).

^cN(H₂) derived from W_{CO} using X_{CO} = 1.6 × 10²⁰ - Hunter et al. (1997).

^dratio of N(H₂) derived from CH (see Table 1) to that derived from CO.

^eX_{CO} in units of cm⁻² [K km s⁻¹]⁻¹ derived from the data in column 6 of Table 1 and column 4 of this table.

REFERENCES

Blitz, L., Bazell, D., & Désert, F.X. 1990, ApJ, 352, L13

Blitz, L. 1991, in The Physics of Star Formation and Early Stellar Evolution, ed. C.J. Lada & N.D. Kylafis (Dordrecht: Kluwer), 3

Dame, T.M., Hartmann, D., & Thaddeus, P. 2001, ApJ, 547, 792

Danks, A.C., Federman, S.R., & Lambert, D.L. 1984, A&A, 130, 62

Federman, S. R. 1982, ApJ, 257, 125

Genzel, R., Downes, D., Pauls, T., Wilson, T.L., & Bieging, J. 1979, A&A, 73, 253

Hjalmarson, Å. et al. 1977, ApJS, 35, 263

Hunter, S.D. et al. 1997, ApJ, 481, 205

Johansson, L.E.B. 1979, *The Galactic Distribution of CH*, Research Laboratory of Electronics and Onsala Space Observatory, Research Report No. 136

Lada, E.A., Bally, J., & Stark, A.A. 1991, ApJ, 368, 432

Lee, H.-H., Bettens, R.P.A., & Herbst, E. 1996, A&AS, 119, 111

Liszt, H. & Lucas, R. 2002, A&A, 391, 693

Magnani, L. & de Vries, C.P. 1986, A&A, 168, 271

Magnani, L. & Onello, J.S. 1995, ApJ, 443, 169

Magnani, L., Hartmann, D., & Speck, B.G. 1996, ApJS, 106, 447

Magnani, L., Onello, J.S., Adams, N.G., Hartmann, D., & Thaddeus, P. 1998, ApJ, 504, 290

Magnani, L., Chastain, R.J., Kim, H.C., Hartmann, D., Truong, T., & Thaddeus, P. 2003, ApJ, 586, 1111

Magnani, L., Zelnik, S., Dame, T.M., & Engebreth, B. 2005, ApJ, submitted

Mattila, K. 1986, A&A, 160, 157

Rachford, B.L. et al. 2002, ApJ, 577, 221

Reach, W.T., Wall, W.F., & Odegard, N. 1998, ApJ, 507, 507

Rydbeck, O.E.H., Kollberg, E., Hjalmarson, Å., Sume, A., & Elldér, J. 1976, ApJS, 31, 333

Scoville, N.Z. & Sanders, D.B. 1987, in *Interstellar Processes*, ed. D.J. Hollenbach & H.A. Thronson, Jr. (Dordrecht, Reidel), 21

Simon, R., Jackson, J.M., Clemens, D.P., Bania, T.M., & Heyer, M.H. 2001, ApJ, 551, 747

Ungerechts, H., Umbanhowar, P., & Thaddeus, P. 2000, ApJ, 537, 221

Viala, Y.P. 1986, A&AS, 64, 391

Weselak, T., Galazutdinov, G.A., Musaev, F.A., & Krelowski, J. 2004, A&A, 949

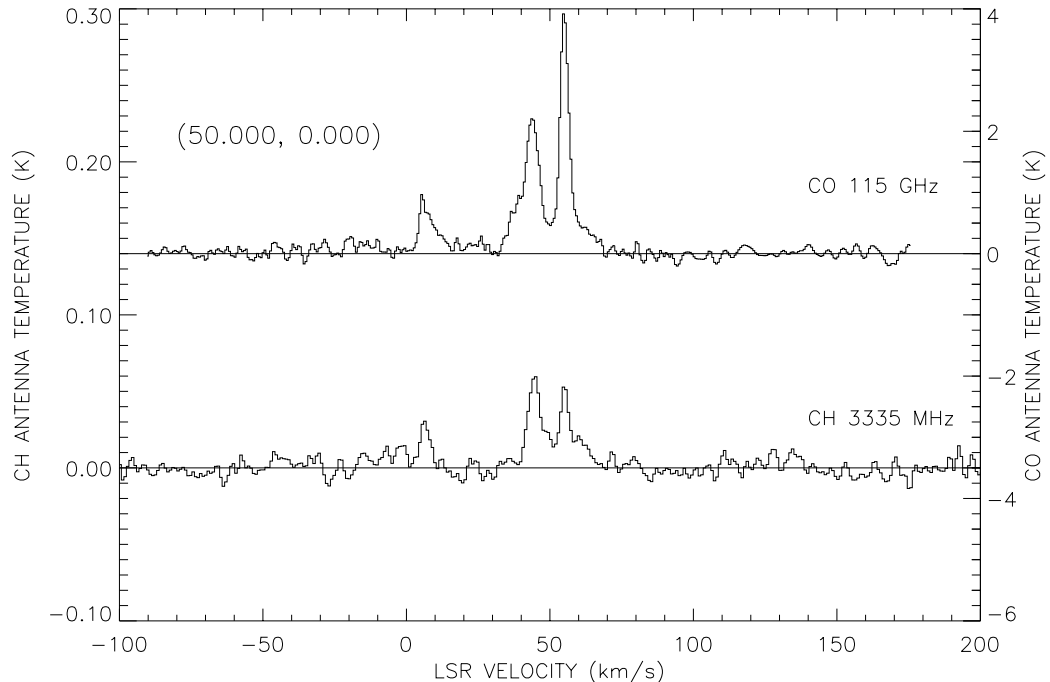


Fig. 1a.— At bottom, spectrum of the CH $^2\Pi_{1/2}$, $J=1/2$, $F=(1-1)$ transition at 3335 MHz for $\ell = 50.0^\circ$, $b = 0.0^\circ$. The beamsize is $9'$ and the velocity resolution is 1.8 km s^{-1} after Hann smoothing. Above, CO(1-0) spectrum from Ungerechts, Umbanhowar, & Thaddeus (2000) for the same position with a beamsize of $8.7'$ and a velocity resolution of 0.65 km s^{-1} .

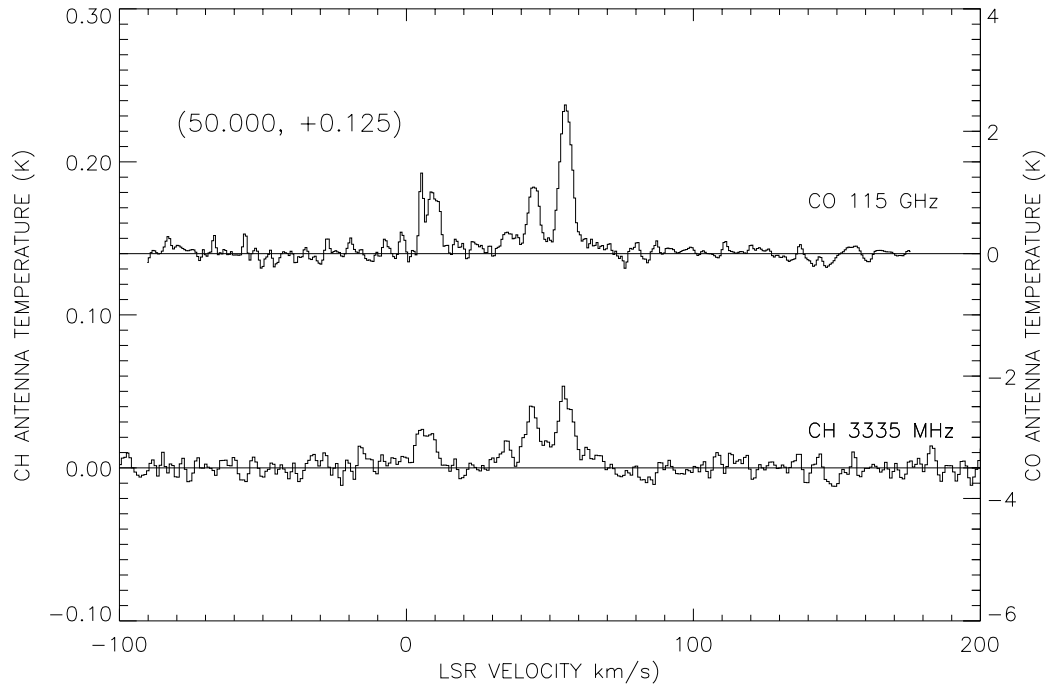


Fig. 1b.— Same as Figure 1a, but for $\ell = 50.0^\circ$, $b = 0.125^\circ$.

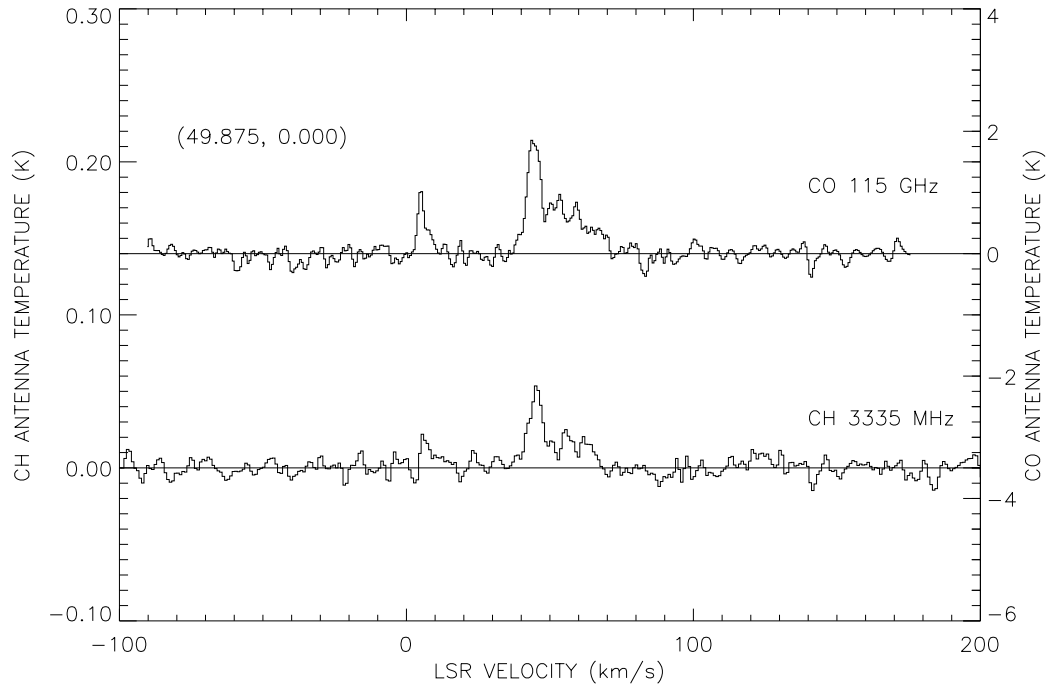


Fig. 1c.— Same as Figure 1a, but for $\ell = 49.875^\circ$, $b = 0.0^\circ$.

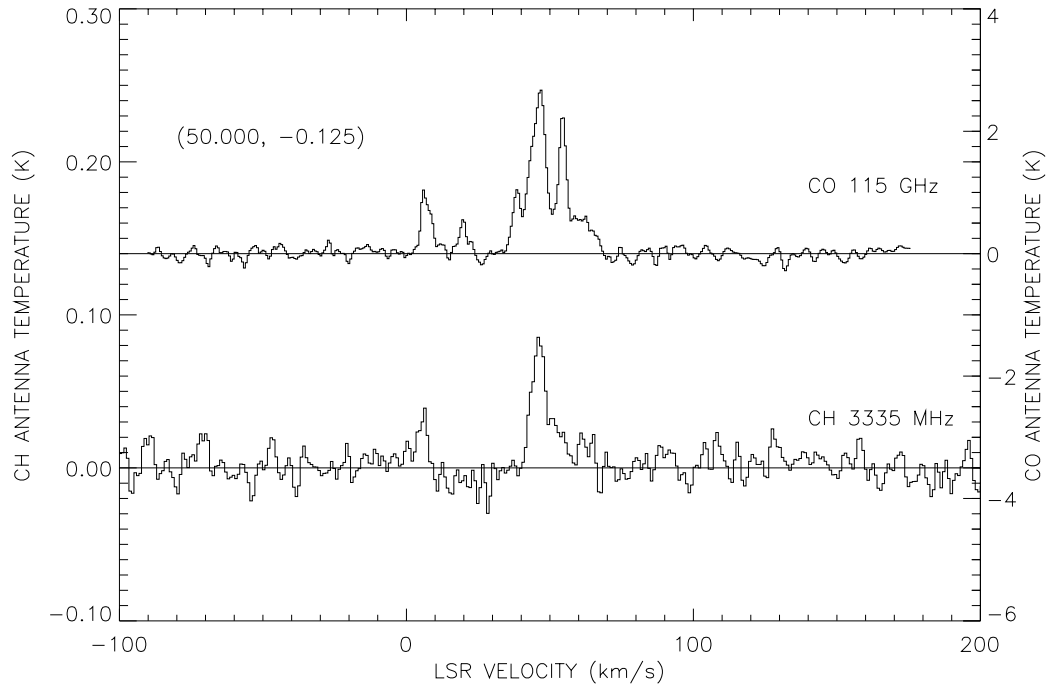


Fig. 1d.— Same as Figure 1a, but for $\ell = 50.0^\circ$, $b = -0.125^\circ$.

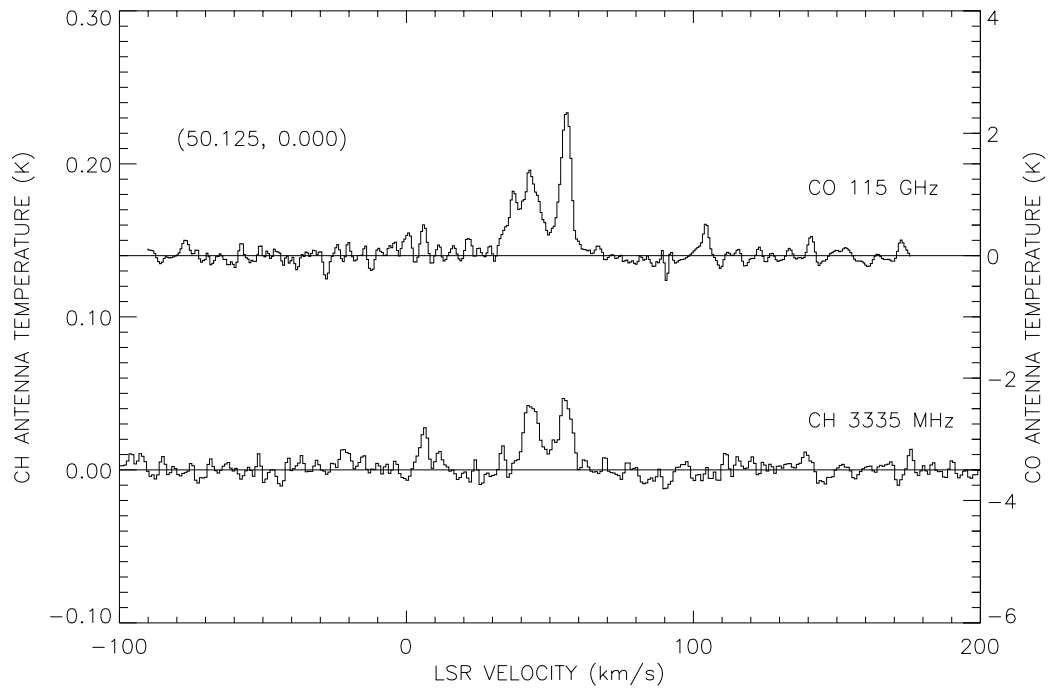


Fig. 1e.— Same as Figure 1a, but for $\ell = 50.0^\circ$, $b = 0.0^\circ$.

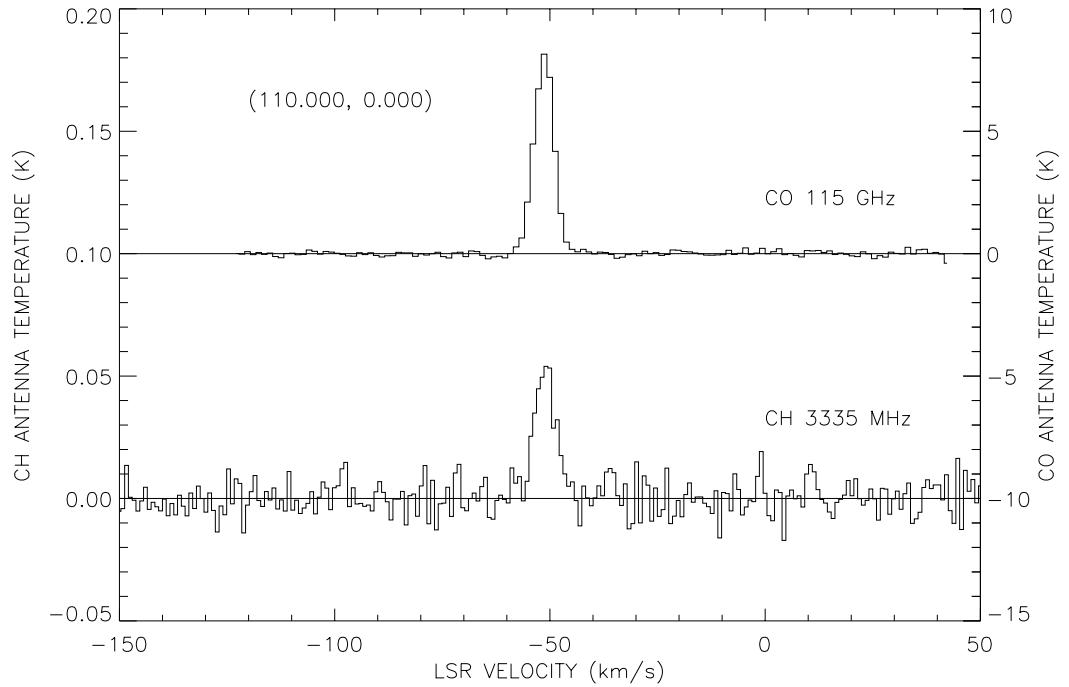


Fig. 2.— Same as Figure 1, but for $\ell = 110.0^\circ$, $b = 0.0^\circ$. The velocity resolution of the CO spectrum is 1.3 km s^{-1} .

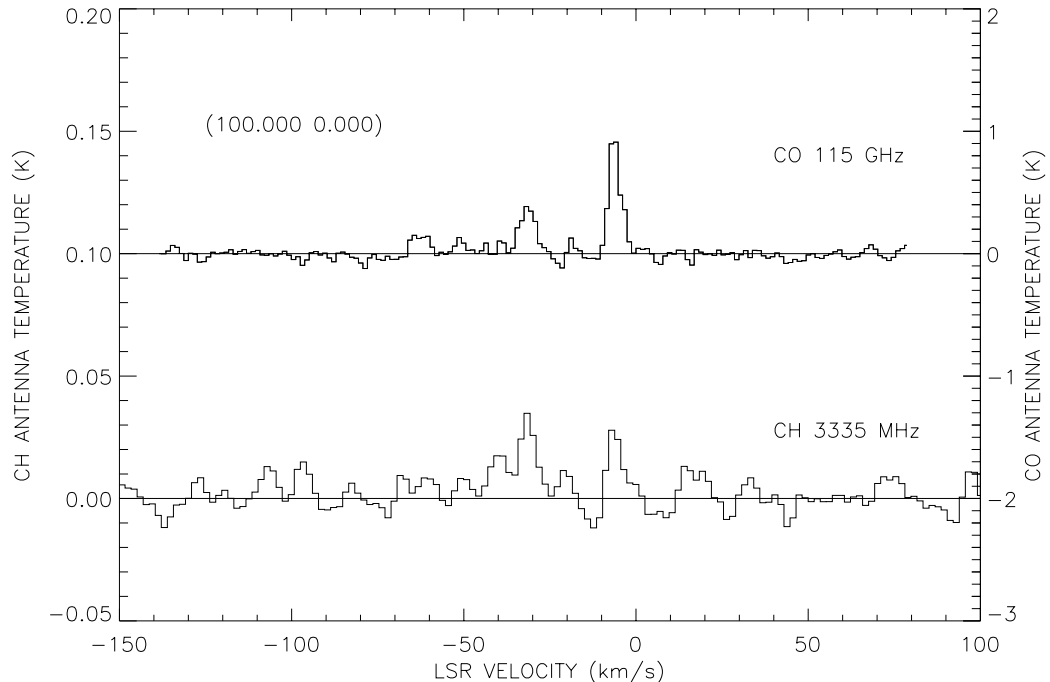


Fig. 3.— Same as Figures 1 and 2, but for the average of the 5 spectra centered on $\ell = 100.0^\circ$, $b = 0.0^\circ$. Both the CO and CH data are averaged over the same 5-point cross. The CH data are Hann smoothed to a velocity resolution of 1.8 km s^{-1} . The CO data are at a resolution of 1.3 km s^{-1} .

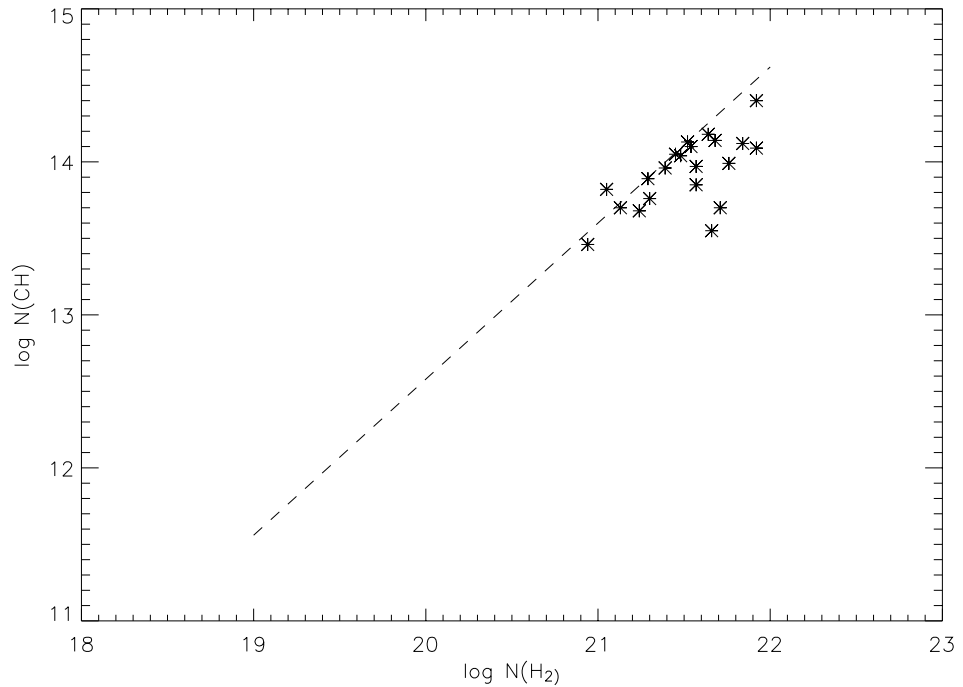


Fig. 4.— Plot of log N(CH) vs. log N(H₂) (column 6 of Table 1 vs. column 5 of Table 2) for comparison with Figure 10 of Mattila (1986). The dashed line is the least squares fit to the translucent and dark cloud data presented by Mattila: $\log N(CH) = 1.02[\log N(H_2)] - 7.82$.

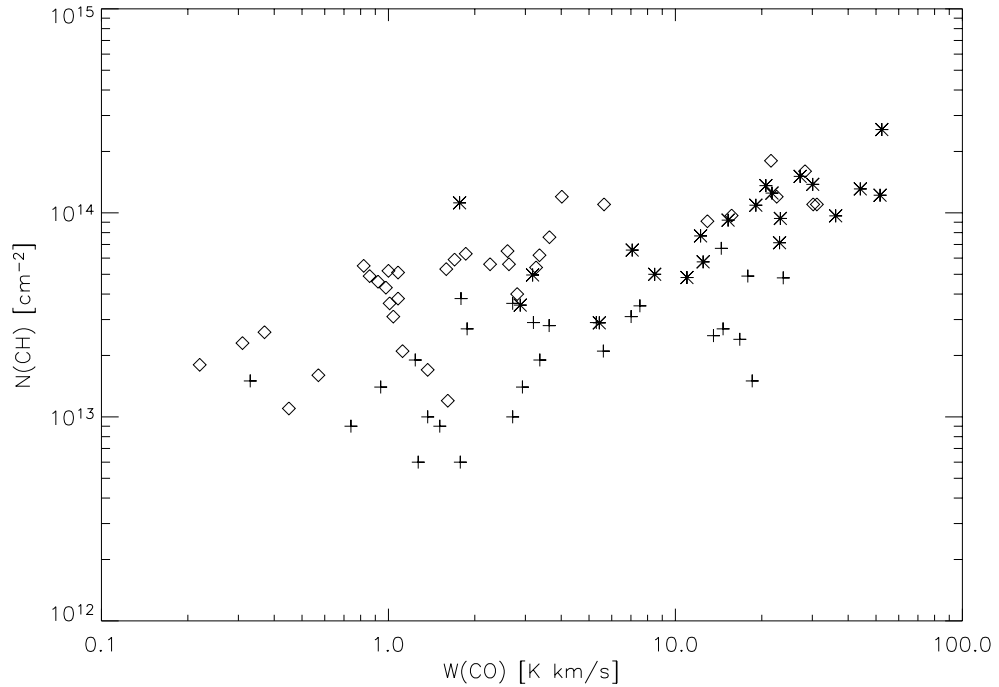


Fig. 5.— Plot of $N(CH)$ vs. W_{CO} for the data presented in this paper (star symbols), and the dark and translucent cloud data from Magnani & Onello (1995) as categorized by Liszt & Lucas (2002). Dark molecular gas is denoted by the diamond symbol, and the plus signs are for translucent gas.

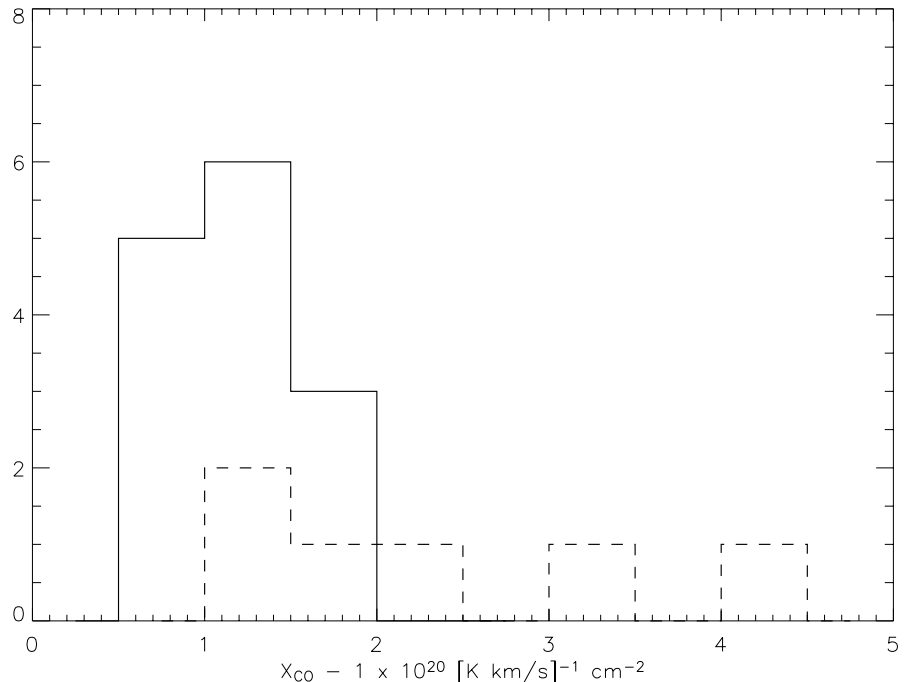


Fig. 6.— Histogram of the X_{CO} values from Table 2 in units of $1.0 \times 10^{20} [\text{K km s}^{-1}]^{-1}$. The solid lines indicate lines of sight through giant molecular clouds and the dashed lines indicate dark and/or translucent lines of sight (see discussion in §5). Not plotted is a dark/translucent data point with an X_{CO} value of 14.5.

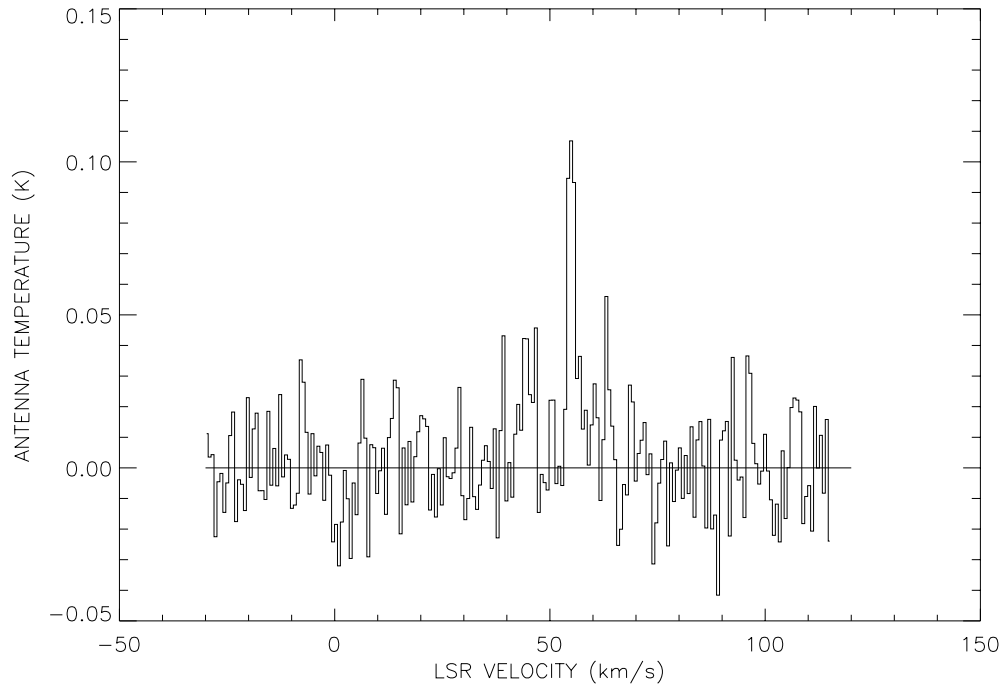


Fig. 7a.— $\text{C}^{18}\text{O}(1-0)$ spectrum of $\ell = 50.0^\circ$, $b = 0.0^\circ$. The beam size is $8.4'$ and the velocity resolution is 0.68 km s^{-1} (see §2 for more details).

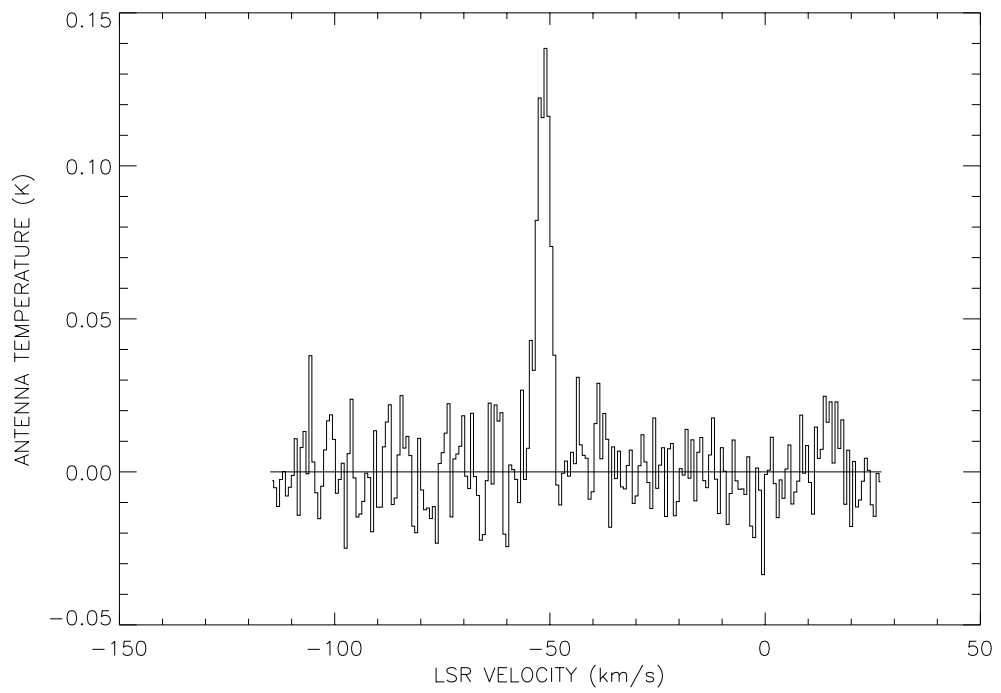


Fig. 7b.— Same as Figure 7a, but for $\ell = 110.0^\circ$, $b = 0.0^\circ$.